Bright CO ro-vibrational emission lines in the class I source GSS 30 IRS1. Probing the inner disk of a young embedded star?

Pontoppidan, K.M.; Schöier, F.L.; Dishoeck, E.F. van; Dartois, E.

Citation
Pontoppidan, K. M., Schöier, F. L., Dishoeck, E. F. van, & Dartois, E. (2002). Bright CO ro-vibrational emission lines in the class I source GSS 30 IRS1. Probing the inner disk of a young embedded star? Retrieved from https://hdl.handle.net/1887/2176

Version:	Not Applicable (or Unknown)
License:	Leiden University Non-exclusive license
Downloaded from:	https://hdl.handle.net/1887/2176

Note: To cite this publication please use the final published version (if applicable).

A&A 393, 585–595 (2002)
DOI: 10.1051/0004-6361:20021056
© ESO 2002

Astronomy & Astrophysics

Bright CO ro-vibrational emission lines in the class I source GSS 30 IRS1

Probing the inner disk of a young embedded star

K. M. Pontoppidan[1], F. L. Schöier[1], E. F. van Dishoeck[1], and E. Dartois[2]

[1] Leiden Observatory, PO Box 9513, 2300 RA Leiden, The Netherlands
[2] Institut d'Astrophysique Spatiale, Bât. 121, Université Paris XI, 91405 Orsay Cedex, France

Received 16 April 2002 / Accepted 12 July 2002

Abstract. We present a 4.5–4.85 μm $R = 5\,000$ spectrum of the low mass class I young stellar object GSS 30 IRS1 ($L = 25\ L_\odot$) in the ρ Ophiuchus core, observed with the infrared spectrometer (ISAAC) on the *Very Large Telescope* (VLT-UT1). Strong line emission from the ro-vibrational transitions of ^{12}CO and ^{13}CO is detected. In total more than 40 distinct lines are seen in the covered region. The line emission is spatially extended and detected up to $2'' = 320$ AU from the central source but is spectrally unresolved ($\Delta v < 30$ km s^{-1}). This is the first time strong emission in the fundamental ro-vibrational band from CO has been observed from an embedded young stellar object. The line fluxes were modeled using a 1-dimensional full radiative transfer code, which shows that the emission is fully consistent with a gas in LTE at a single well constrained temperature ($T = 515 \pm 10$ K). Furthermore, the ratios between lines from the two detected isotopic species of CO show that the ^{12}CO lines must be optically thick. However, this is inconsistent with the observed spatial extent of the emission, since this implies such low CO column densities that the lines are optically thin. A likely solution to the discrepancy is that the lines are emitted by a smaller more dense region and then scattered in the bipolar cavity present around the central star. This gives a rough estimate of the total molecular gas mass of 1–100 $M_\oplus$ and a physical extent of ~20–100 AU. We propose that the most likely origin of the line emission is post-shocked gas in a dense dissociative accretion shock from the inner 10–50 AU of a circumstellar disk. The presence of a shock capable of dissociating molecules in the disk will have implications for the chemical evolution of disks around young low mass stars.

Key words. line: formation – radiative transfer – stars: formation – ISM: individual objects: GSS 30 IRS1 – ISM: molecules⋆

1. Introduction

The innermost 50 AU of the circumstellar environments around embedded young stellar objects is poorly constrained observationally due to the large extinction through the embedding material ($A_V > 20$ mag) and the small angular size ($<1''$) of the region. The usual molecular probes in the millimeter-submillimeter region are not effective for the temperatures ($T > 200$ K) and densities ($n_{\mathrm{H_2}} > 10^7$ cm^{-3}) thought to be present. However, an understanding of the processes taking place in this regime is essential to obtain a complete picture of the process of accretion and the driving of outflows from low mass protostars as well as the early chemical and physical evolution of circumstellar disks.

One of the most effective probes of warm dense gas is through emission in molecular ro-vibrational transitions. The most common bands readily available from ground-based facilities are the CO overtones and H_2 fundamental bands around 2.2 μm (e.g. Reipurth & Aspin 1997) and the fundamental transitions of CO in the M-band around 4.7 μm. Also emission from very hot water gas (~2000 K) near 2.29 μm has been reported toward a few sources (e.g. Najita et al. 2000). Since the upper levels of these transitions lie at temperatures of up to a few thousand Kelvin, they probe hot gas with temperatures between 100 and 1000 K, making them ideal to study the region of interaction between disk, protostar, accretion and outflow. With the new generation of sensitive ground-based high resolution spectrometers for the 3–5 μm region an efficient window has been opened for the detailed study of the CO ro-vibrational lines toward embedded young stellar objects (YSO). The past generation of instruments was suitable to either observe a low resolution spectrum with a fairly wide spectral range (e.g. Teixeira et al. 1998) or a high resolution echelle spectrum with a very narrow spectral range (e.g. Carr et al. 2001). The main exception are the Fourier Transform Spectroscopy (FTS) observations of Mitchell et al. (1988, 1990), who observed a number

Send offprint requests to: K. Pontoppidan,
e-mail: pontoppi@strw.leidenuniv.nl

⋆ Based on observations obtained at the European Southern Observatory, Paranal, Chile, within the observing program 164.I-0605.

of high-mass stars in the entire M-band at high spectral resolution ($R > 10^6$), but such studies are limited to the brightest objects. VLT-ISAAC has a large instantaneous spectral range in the M-band (0.237 μm), which combined with a medium resolution of $R = 5\,000-10\,000$ and a limiting magnitude of $M \sim 10$ allows the entire fundamental band of gaseous CO of a wide range of young stars to be observed in a short time, including low mass stars down to a few tenths of a solar mass in the nearest star-forming clouds.

The embedded stars studied so far in CO ro-vibrational bands have showed mostly lines in absorption (Mitchell et al. 1990; Boogert et al. 2000, 2002) implying that the warm CO gas is seen in front of a bright infrared continuum, produced by hot dust close to the central object. The fundamental CO lines are usually only seen in emission towards more evolved sources characterized by a class II type spectrum where a circumstellar disk is directly visible (Carr et al. 2001; Blake et al. 2002). CO overtone bandhead emission at 2 μm has been observed in emission toward a few intermediate mass pre-main sequence stars (Thompson 1989; Najita et al. 1996) and T Tauri stars (Carr 1989), and has been associated with hot gas ($T \sim 1\,500-5\,000$ K) located within a fraction of an AU in a Keplerian disk.

We present here the peculiar 4.5−4.8 μm spectrum of the illuminating source IRS1=Elias 21 of the bipolar reflection nebula GSS 30 located in the core of the ρ Ophiuchus molecular cloud at a distance of 160 pc. It has been classified as a low mass class I YSO from its spectral energy distribution (SED) (Grasdalen et al. 1973; Elias 1978; Wilking et al. 1989) and low bolometric luminosity ($L_{\rm bol} = 21-26\ L_\odot$, Greene et al. 1994; Bontemps et al. 2001). Extensive polarimetric studies in the H and K band of the reflection nebula have shown that the source is surrounded by a large (∼2000 AU) disk-like envelope and a smaller circumstellar disk of ∼150 AU, which are inclined about 25° away from the plane of the sky, i.e. close to edge-on (Chrysostomou et al. 1996, 1997). The high degree of linear polarization (up to 50%) as well as the presence of circular polarization imply that the light coming from the reflection nebula must have been multiply scattered, before heading into the line of sight.

Two other sources (IRS2 and IRS3) are present toward the K-band reflection nebula (within 20″ of IRS1). IRS2 has a class III SED and is probably a more evolved star (André & Montmerle 1994). IRS3 has a class I SED, but is much fainter than IRS1 in the near-infrared. It has a bolometric luminosity of 0.13 $L_\odot$, (Bontemps et al. 2001). IRS3 shows strong 6 cm emission (see Leous et al. 1991, where IRS3 is designated LFAM 1).

The presence of a molecular outflow has not been firmly established. High velocity red- and blue-shifted CO millimeter emission to the south of GSS 30 has previously been reported by Tamura et al. (1990), but since both lobes are located to the south of the infrared source, the gas is likely to be associated with the VLA 1623 jet, which is passing only 30″ to the SW of IRS1. Using millimeter interferometric line data, Zhang et al. (1997) find evidence for a spherical expansion of the core surrounding the three sources in GSS 30. In addition, the inner region of the core seems to be cleared, which is indicative of a young outflow. This is additionally supported by the presence of variable unbound water maser emission from within 0.″3 of IRS1 (Claussen et al. 1996).

2. Observations

The observations of GSS 30 IRS1 were carried out using the long wavelength (LW) medium resolution mode on the Infrared Spectrometer And Array Camera (ISAAC) mounted on the Very Large Telescope (VLT-UT1) at the Paranal Observatory on September 3, 2001. The detector for 3−5 μm observations is a 1K×1K Aladdin InSb array, which allows a spectral coverage of 0.237 μm per setting in the M-band with a spectral resolution of up to $R = 10\,000$. The detector resolution in the spatial direction in the spectroscopic modes is 0.″148/pixel. The spectrum of this source was taken as a part of a large program to study ices and gas around young low mass stars (van Dishoeck et al. 2001).

The data were obtained under excellent photometric conditions in service mode with ∼0.″3 infrared seeing and ≲10% humidity which gave a very stable atmosphere. The frames were both chopped and nodded along the slit with a 15″ chop throw. The 0.″6 slit was used in two settings for 20 min per setting yielding a final signal to noise ratio on the continuum of the extracted spectrum ranging from 50 to more than 100 over a spectral range from 4.5 μm to 4.82 μm and with a spectral resolution of $R = 5000$.

The standard star BS6084 (B1III) was observed at air masses between 1.2 and 1.5 immediately before GSS 30 for removal of telluric features, while the source was observed at air masses between 1.5 and 2.1. Because the source was already descending at the time of observation, it was not possible to observe source and standard at the same airmass as is otherwise of importance in order to obtain a good telluric subtraction. However, due to the exceptional stability of the atmosphere through most of the night we were able to correct for the airmass difference using a simple Lambert-Beer law, which states that the depth of the atmospheric lines scales exponentially with the airmass. The final corrected spectrum turned out to be of acceptable quality in spite of the airmass difference. Our experience is that it is crucial to use a B star or an early A star as the standard because many narrow intrinsic stellar lines become visible in the 3−5 μm region for spectral resolutions better than ∼1000 if an F or later type star is used.

The spectrum was reduced with IDL routines using standard methods appropriate for chopped and nodded infrared spectroscopy. Bad pixels were removed, the frames were distortion corrected using the telluric features in a star-trace map as reference, and AB nodded pairs were subtracted to remove the long time scale differences which the chopping is not capable of removing. The spectra were extracted by integrating over a spatial width determined by the positions along the slit where the signal drops below the 3σ level. The raw spectrum was then ratioed by the standard after applying an optimized shift and airmass correction. In the final spectrum, the points where telluric residuals are apparent have been removed, including the region short-wards of 4.55 μm, where atmospheric CO_2 lines render the spectrum useless. The final result is shown in Fig. 1.

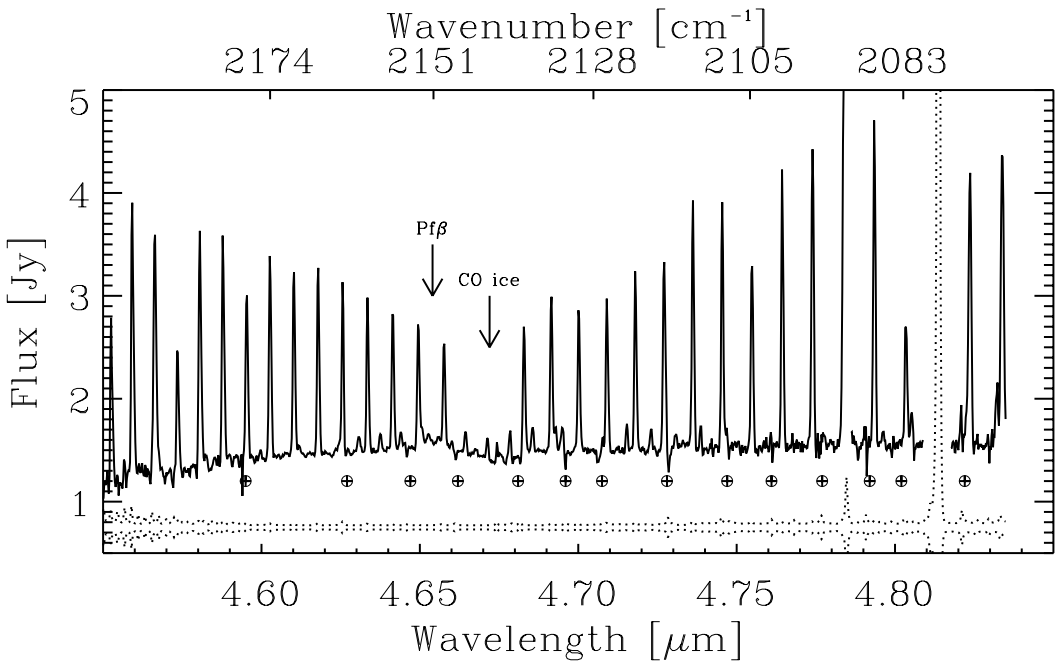

Fig. 1. The VLT-ISAAC M-band spectrum of GSS 30 IRS1 at $R = 5000$. The statistical (3σ) error is shown below the spectrum. Note that this error does not take the systematical errors introduced by variable telluric absorption into account which dominate in some parts of the spectrum. Since the peaks in the statistical error indicate deep atmospheric absorption they can be used to locate where telluric residuals might be interfering with the intrinsic spectrum. The telluric residuals which are exceeding the noise are marked with a ⊕ and are seen to correlate well with the peaks in statistical error.

The CO ro-vibrational lines in the spectrum are red-shifted with ∼20 km s^{-1} due to the systemic velocity of the Earth relative to the source, which means that there is a significant overlap between intrinsic CO lines and telluric absorption by CO. In spite of this, the telluric division is very good, especially when taking the unfavorable airmasses of source and standard into account. A few residuals from telluric ^{12}CO absorption are visible and are marked in the final spectrum. Since the resolution of our spectra is 60 km s^{-1}, none of the features in the source are unaffected by the telluric lines. At higher resolution ($R > 20\,000$) the telluric lines may saturate, thereby forcing a division by zero when ratioing with the standard and resulting in a loss of information in the affected pixels. At sufficiently high resolution, this will not be a problem since the narrow telluric lines will often be completely offset from the intrinsic lines. However, at a resolution of 5000, the typical telluric line has a depth which is only a fraction of the intrinsic continuum allowing a significant signal to be present in the standard spectrum even in the center of a telluric line and only very few lines are partially or completely lost due to saturated telluric lines.

By measuring the strength of the small residuals from telluric lines of species not intrinsically present in the source spectrum, the systematic uncertainty in the source lines is estimated to be less than 15%. The statistical uncertainty for the brighest lines is typically a few %, while the faintest lines are 3σ detections. The spectrum was wavelength calibrated relative to the telluric lines and flux calibrated relative to the standard star. The wavelength calibration of high resolution M-band spectra is very accurate due to the large number of telluric lines, and a conservative estimate for the precision is ∼5 km s^{-1} over the entire spectrum. Indeed, the standard deviation of the line center velocities given in Table 1 is 4.2 km s^{-1}. Due to the difference in airmass between standard and source, we estimate the systematic uncertainty in absolute flux calibration to be ∼30%. Since the bright lines are typically most severely affected by telluric residual, all line fluxes have total uncertainties with values between 15 and 50%. The exact uncertainty for each line is difficult to estimate and we consequently adopt a value of 30% for all lines.

3. Results

3.1. Signatures of hot CO gas

It is evident that the M-band spectrum of GSS 30 is dominated by strong emission lines from the ro-vibrational ($v = 1$–0) transitions of ^{12}CO gas. R- and P-branch lines within the observed spectral range are detected up to $J = 15$ and $J = 18$, respectively. The lines are all unresolved at a resolution of $R = 5000$, which gives an upper limit to the intrinsic line width of 30 km s^{-1}. No apparent decrease in line intensity is seen towards higher rotational quantum numbers, so observing the source in the entire M-band will clearly detect more lines. The brightest lines reach peak fluxes of more than 200% of that of the continuum. However, since none of the lines are resolved, this is only a lower limit to the peak flux. Fainter detected features include ^{13}CO $v = 1$–0 lines as well as ^{12}CO $v = 2$–1 lines. The fact that the observed gas has a population excited to the second vibrational level already indicates that the gas is at least

warmer than a few hundred K. The ^{12}CO v = 1–0 lines have intensities of order 2×10^{-13} erg s^{-1} cm^{-2}, the ^{13}CO v = 1–0 and ^{12}CO v = 2–1 lines being 1–2 orders of magnitude fainter. The line fluxes of all unblended lines were extracted by fitting a Gaussian as well as a first order polynomial to the local continuum. After subtraction of the continuum, the fluxes were derived by integrating the spectrum in a 3σ region around the line.

The extracted fluxes of all unblended lines are given in Table 1. Many of the faint lines are completely blended with the bright lines, but it was still possible to extract 12 ^{13}CO v = 1–0 lines and 4 ^{12}CO v = 2–1 lines, which is sufficient to constrain the most important parameters of the emitting gas.

In addition to the CO emission lines, a faint 4.67 μm CO ice feature is visible. Since the feature is partly filled by the bright ^{12}CO $P(1)$ line it is not possible to obtain a well-defined ice profile. For the same reason the affected emission line is not included in the analysis and modeling. There is also a very broad ($FWHM \sim 500$ km s^{-1}), 4.65 μm Pfund β hydrogen recombination line visible, although with the bright CO lines superposed.

Finally, the H_2 0 – 0 S(9) line is detected with an integrated line flux of $2 \pm 1 \times 10^{-14}$ erg s^{-1} cm^{-2}, signifying the presence of hot (>1000 K) molecular hydrogen or possibly shock-excited gas.

3.2. Size of the emitting region

In order to determine the parameters of the line emitting gas unambiguously, the size of the emitting region must be known. The *FWHM* of the continuum in the spatial direction is about 0.″5, which is consistent with the seeing throughout the observation. However, the lines appear to be spatially resolved, although most of the line flux is centered on the source. The wings of the spatial profile of each line extend up to 2″ away from the central source along the slit. This is illustrated in Fig. 2, which shows the normalized average of the spatial profile of the lines, with the normalized average of the continuum profile subtracted. It is evident that the line emission is resolved and detected to a distance of more than 320 AU from the central source. There is also an indication that the northern part of line emission is stronger than the southern part, which agrees with the morphology seen in the *L*-band image of IRS1 shown in Fig. 3.

This extension suggests that the line emission is associated with the scattering nebula and is not coming directly from the central source. Since the continuum is less spatially extended than the line emission, the line emitting region appears to be spatially distinct from the continuum emitting region. Possible interpretations are that the line emission can be coming from gas present in the bipolar lobes (e.g. an outflow), from resonance scattering of continuum emission or from scattering of lines emitted closer to the star. Each of these possibilities will be discussed in detail below as the size of the emitting region depends strongly on the scenario.

Table 1. Integrated CO line fluxes toward GSS 30 IRS1.

Transition	Line flux [10^{-13}erg cm^{-2} s^{-1}]	Heliocentric velocity [km s^{-1}]
^{12}CO v = 1–0		
$R(0)$	1.16	−16
$R(1)$	1.27	−13
$R(2)$	1.64	−11
$R(3)$	1.74	−11
$R(4)$	1.69	−10
$R(5)$	2.08	−11
$R(6)$	2.16	−11
$R(7)$	2.49	−10
$R(8)$	2.10 [a]	−5
$R(9)$	2.78	−10
$R(10)$	3.14	−14
$R(11)$	1.46 [a]	−4
$R(12)$	3.85	−14
$R(13)$	3.42	−14
$P(2)$	1.59	−11
$P(3)$	1.58	−11
$P(4)$	1.62	−12
$P(5)$	1.73 [a]	−12
$P(6)$	1.94	−8
$P(7)$	2.76 [a]	−3
$P(8)$	2.84	−9
$P(9)$	2.42	−10
$P(10)$	2.16	−8
$P(11)$	2.95	−2
$P(12)$	3.37	−4
$P(14)$	3.40	−7
^{12}CO v = 2–1		
$R(6)$	0.08	−17
$R(7)$	0.10	−12
$R(8)$	0.10	−14
$R(9)$	0.07	0
^{13}CO v = 1–0		
$R(3)$	0.19	−11
$R(4)$	0.18	−11
$R(5)$	0.24	−14
$R(6)$	0.29	−11
$R(10)$	0.30	−15
$R(11)$	0.43	−14
$R(12)$	0.23	−14
$R(13)$	0.27	−10
$R(16)$	0.17 [a]	−15
$R(17)$	0.23	−3
$R(18)$	0.19	−19
$R(21)$	0.02	−15

[a] This line is severely affected by telluric residual.

4. Models

4.1. Optically thin LTE models

As a simple first approximation, the extracted line intensities were fitted with a one-temperature optically thin LTE model. The molecular data were taken from the HITRAN database (Rothman et al. 1998) and the relative line intensities were calculated directly from a Boltzmann level population

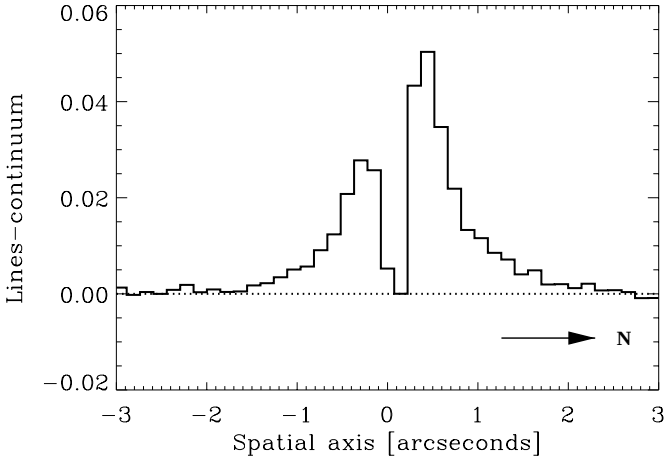

Fig. 2. Spatial cross section of the resolved line emission. The spatial distribution of the emission (along the slit) is shown averaged over all ^{12}CO v = 1–0 lines with the continuum spatial profile subtracted. The line spatial profile was normalized to the continuum profile to show that the lines are detected over a larger region than the continuum. The direction to the north on the sky is indicated on the figure.

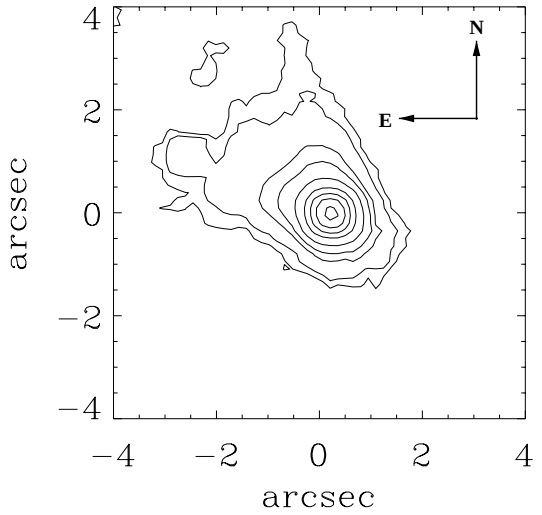

Fig. 3. The 3.21 μm acquisition image of the reflection nebula surrounding GSS 30 IRS1. The north-eastern lobe is clearly visible and also extended emission from the south-western lobe is resolved. The slit was centered on (0, 0) and directed north-south. The contours are roughly logarithmic with the lowest contour at values two orders of magnitude smaller than the highest contour.

distribution. The two parameters of the model, the gas kinetic temperature and the CO column density, should be well constrained in the optically thin limit. If only the ^{12}CO v = 1–0 transitions are used, an optically thin model is to some extent degenerate in the two parameters. This degeneracy is due to the fact that the populations in the vibrationally excited levels are much more sensitive to temperature changes in the 400−800 K range than the rotational level populations. Since lines from two species are available, the degeneracy is broken. It is reasonable to assume that the emission from both species is coming from the same mass of gas, and that the ^{12}C/^{13}C-ratio is close to 60 (e.g. Bensch et al. 2001).

This model is not able to provide a good fit to the entire line spectrum. However, from Fig. 4 it is evident that the faint ^{13}CO v = 1–0 and ^{12}CO v = 2–1 lines can be simultaneously fitted with a single temperature gas in the optically thin limit. The model lines of ^{12}CO v = 1–0 are however an order of magnitude too bright. Excluding the ^{12}CO v = 1–0 lines from the fit yields a well-constrained temperature of 515 ± 25 K and a total ^{12}CO column density of $4 \pm 1 \times 10^{14}$ cm^{-2}. Since the fit includes lines from both CO isotopic species, we conclude that it is unlikely that the apparent discrepancy between the ^{12}CO v = 1–0 and ^{13}CO v = 1–0 lines is due to a deviation from the normal interstellar ratio. The simplest explanation is that the ^{12}CO v = 1–0 lines are optically thick, while the rest remain optically thin. This would conveniently prevent us from seeing the whole column of ^{12}CO and could possibly lower the line intensities enough to explain the data. However, the fundamental ro-vibrational transitions of ^{12}CO do not produce optically thick lines for column densities less than $\sim 10^{17}$ cm^{-2}, which is still 250 times more than the simple model dictates. Thus the optically thin LTE model is internally inconsistent.

4.2. Results of the full radiative transfer model

In order to quantify the discrepancy more accurately, we computed the full radiative transfer for a single temperature static envelope in LTE. For simplicity a spherical geometry was assumed since the results are not very sensitive to geometry. The size and density of the emitting region cannot be constrained by the model, so the quantities fitted were the single gas temperature and the column density of the gas, by keeping the size fixed at the observed 4″.

Furthermore, it is assumed that the line intensity is independent of the underlying continuum. This last assumption may not be completely valid, since the CO lines could be present in absorption in the continuum before the lines from the emitting gas are superposed. The effect of this would be to lower the line peak flux with maximally the continuum flux level. Since the lines are completely unresolved, the true peak flux of the lines is higher than that observed. The observed peak flux of the ^{12}CO v = 1–0 lines is 2–3 times higher than the continuum flux, so we conclude that this effect can only effectively lower the intensity of these lines with a small fraction at most. The fainter lines can be significantly suppressed by absorption in the continuum if they are optically thick, but this would only increase the discrepancy between the bright and faint lines. Also, if the absorption lines are significantly broader than the superposed emission lines, the observed line intensities could be sufficiently suppressed. However, since we have no possibility of constraining this with the present data, we assume that the possible absorption lines and the emission lines have similar intrinsic widths, i.e. the contribution from absorption in the continuum is negligible. Higher resolution spectra may clarify the matter.

The ^{13}CO v = 1–0 lines were first fitted independently of the ^{12}CO v = 1–0 and ^{12}CO v = 2–1 lines. The model confirms that the two sets of lines cannot be fitted simultaneously, although each set is consistent with a single temperature gas.

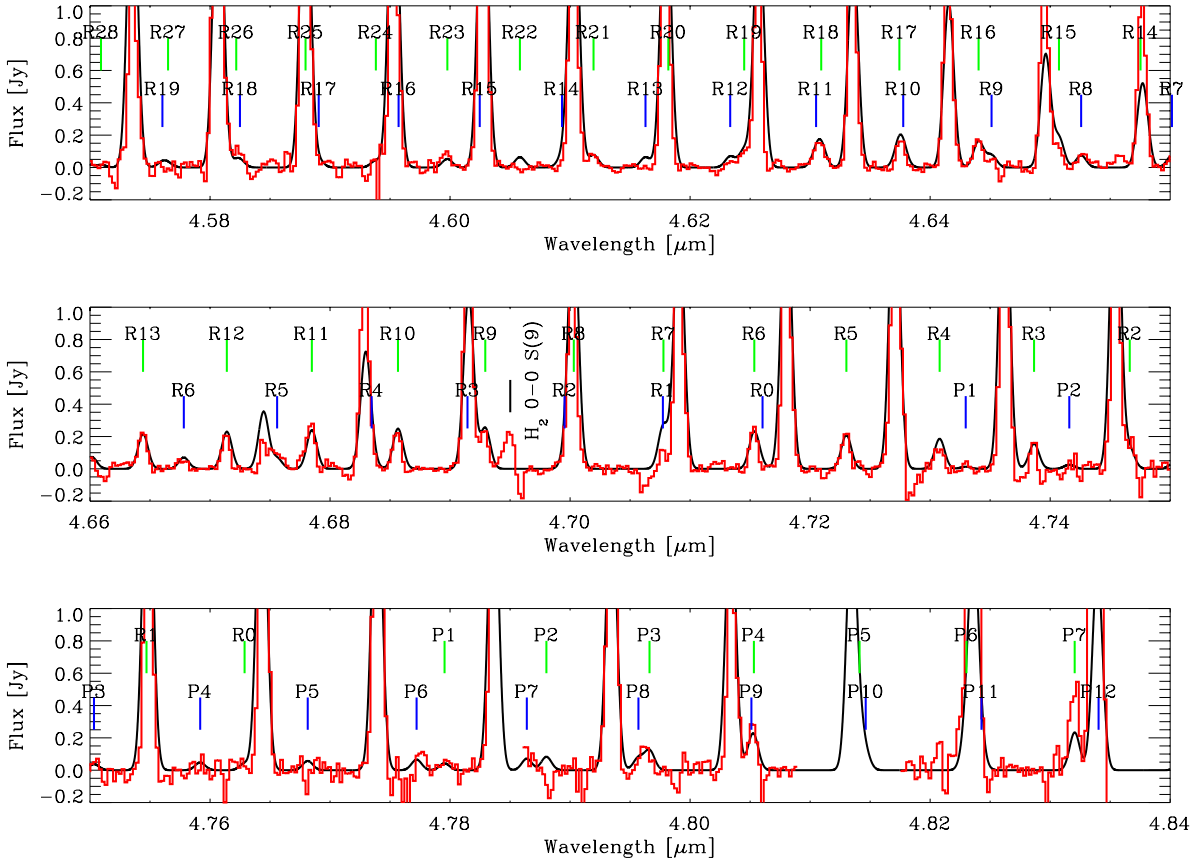

Fig. 4. Continuum subtracted spectrum of GSS 30 IRS1. Top row of line identifications show the ^{13}CO v = 1–0 lines. Bottom row of identifications show the ^{12}CO v = 2–1 lines. The data have been over-plotted with the optically thin LTE model spectrum. The model ^{12}CO v = 1–0 line fluxes have been divided by a factor of 7 for clarity and to illustrate the optical depth effects.

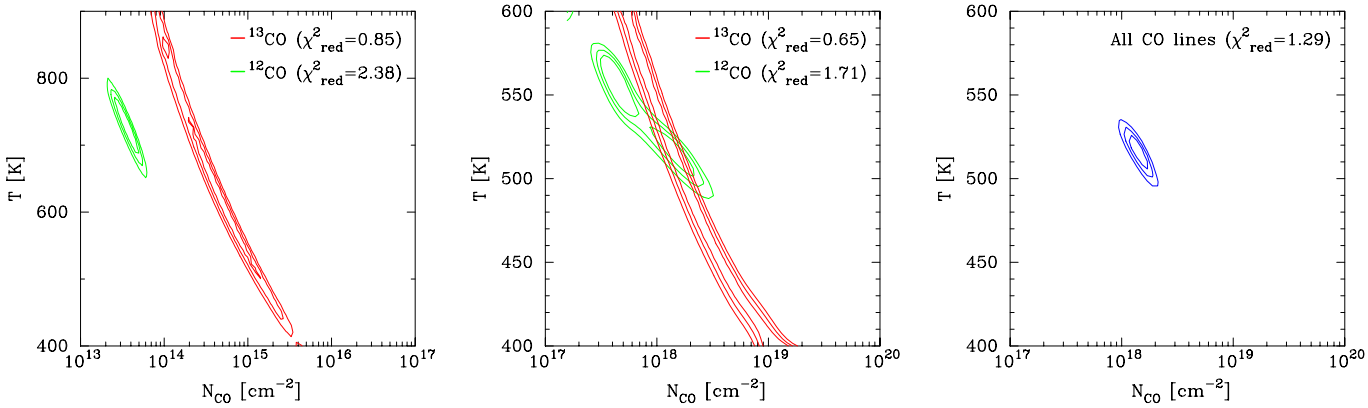

Fig. 5. χ^2 maps of the best fitting models. Left panel: the ^{12}CO v = 1–0 and ^{12}CO v = 2–1 lines plotted against the ^{13}CO v = 1–0 lines without the assumption of scattering, in which case the sets of well-fitting parameters do not overlap. Middle panel: χ^2 contours for the ^{12}CO v = 1–0 and ^{12}CO v = 2–1 lines over-plotted by contours for the ^{13}CO v = 1–0 lines, but now with a scattering factor $\epsilon = 1.4 \times 10^3$. Right panel: The weighted sum of the two χ^2 maps from the middle panel. The contours show in all the maps the 1, 2 and 3σ levels.

There is a certain degeneracy in the two free parameters, especially in the ^{13}CO lines, and the model gives a one-dimensional family of good fits for each species. However, the two families do not overlap for the observed line intensities. Fitting the ^{12}CO v = 1–0 and the ^{12}CO v = 2–1 lines simultaneously yields poorer fits than fitting them separately. All the lines are in the extreme optically thin limit with typical values of $\tau \simeq 10^{-3}$ for the ^{12}CO v = 1–0 lines. The discrepancy between the ^{12}CO v = 1–0 and ^{12}CO v = 2–1 lines may be due to non-LTE effects, reflecting that the rotational temperature $T_{\rm rot}$ and the vibrational temperature $T_{\rm vib}$ are not equal. However, non-LTE effects cannot explain why the ^{12}CO v = 1–0 to ^{13}CO v = 1–0 line ratios differ with almost an order of magnitude from the predictions of the simplest LTE model, since

the excitation structures of different isotopic species must be almost identical.

To explain the data, we propose that all the observed line emission has been scattered by dust in the bipolar cavity seen in the near-infrared. The scattering efficiency is very low at 4.7 μm, and thus only a small fraction of the original line emission will be scattered into the line of sight. This means that the line intensities from the emitting region and consequently the column densities can reach much larger values than those previously suggested by the model. To test this hypothesis, we adopted a factor, $\epsilon = S \times (\pi R^2)/\Omega$, which accounts for our lack of information about the true solid angle of the emitting region Ω, and the ratio of intrinsic line flux to line flux scattered into the line of sight, S . R is the observed angular radius of the emitting region, which is taken to be $R = 2''$. Absolute upper and lower bounds to the size of the emitting region are given by the natural conditions $S > 1$ and $\Omega < \pi R^2$. Decreasing the size of the emitting region will increase the column densities, but since line emission is observed far from the source, we cannot explain the entire discrepancy with a smaller emitting size. To recover the original flux it is necessary to multiply the observed values with this factor. Multiplying all observed line intensities with a sufficiently large factor will allow the ^{12}CO $v = 1$–0 lines to become optically thick. We are able to constrain the scattering factor in the model by demanding a simultaneous fit to all the lines.

The best fitting value of the scattering factor is $\epsilon = 1.4 \times 10^3$ with a reduced χ^2 of 1.29, which gives a well-constrained single temperature LTE gas at 515 ± 10 K and $N(\mathrm{CO}) = 1.5 \pm 0.5 \times 10^{18}$ cm^{-2}, as indicated in Table 2. With an extent of the emitting region of 4″ an upper limit to the total gas mass of 200 $M_\oplus$ is found. Since the total gas mass scales with $\Omega^{0.5}$ an absolute lower limit to the mass is 1.3 $M_\oplus$ with a diameter of the emitting region of 0.19″ = 30 AU, assuming that $S = 1$ and ignoring that line emission is observed to much larger distances from the central source. Since S must be significantly less than unity, the total mass is most likely significantly larger than the lower limit. It is not necessary to invoke any non-LTE effects to obtain a nearly perfect fit to all the observed lines and the assumption of LTE holds such that $T_{\mathrm{rot}} = T_{\mathrm{vib}}$. The χ^2 maps of the best-fitting models are shown in Fig. 5.

It is possible to make an estimate for an absolute lower limit to the grain size by assuming $S = 1$. In this case the scattering efficiency, $Q_{\mathrm{sca}} > \epsilon$, since it is not possible to scatter more light into the line of sight than out of it. This happens for silicate grain sizes larger than 0.2–0.3 μm (Draine & Lee 1984; Draine 1985). As a consequence the grains must be large, perhaps as large as 1 μm, which is expected for grain growth in dense media (Pendleton et al. 1990). On the other hand, the lower limit on the size of the scattering grains does not fit with the polarization maps of the GSS 30 nebula. Chrysostomou et al. (1996) finds that grains larger than 0.35 μm are inconsistent with the variation of linear polarization with wavelength. However, the polarization was mapped on a much larger angular scale than the size of the nebula at 4.6 μm, so the discrepancy may be explained by grain growth within a few hundred AU of the central source.

4.3. Other scenarios and pumping mechanisms

One way of avoiding the scattering assumption entirely may be to apply a two-temperature model to the data. In this scenario a small part of the gas close to the central source with a kinetic temperature of ~1000 K would be responsible for the ^{12}CO $v = 2$–1 lines as well as part of the high J lines of the $v = 1$–0 lines, while a massive outer component at ~200 K would dominate the emission in the low J lines. The scattering assumption would not be needed since the ^{12}CO $v = 1$–0 lines require a much higher column density to create the observed line intensity at 200 K compared to 500 K and will thus more readily become optically thick. We applied a two-temperature model by requiring that the total column density must be the same as that determined by the single-temperature model. This is reasonable because the optical depth of the lines is given by the ratio between the ^{12}CO and ^{13}CO lines independently of ϵ and therefore must be conserved. As in the single-temperature model three parameters are varied, namely the two temperatures and the ratio of the column density between the components. In other words, ϵ is exchanged as a free parameter with a second temperature, thus keeping the number of free parameters constant.

The ^{13}CO lines can be fitted well within the two-temperature model, although the parameters are somewhat degenerate in the same way as in the single temperature model. However, it was not possible to fit the ^{12}CO lines within this scenario, with the best reduced χ^2 being of order 10. Furthermore, there is a preference towards a single low temperature in the ^{12}CO lines which is inconsistent with the ^{13}CO lines. Inclusion of all lines gives no meaningful fits within the parameter space. The explanation is that it is not possible to combine the ^{12}CO $v = 2$–1 and the ^{12}CO $v = 1$–0 lines, since the high temperature component easily produces too much $v = 1$–0 emission in order to fit the $v = 2$–1 emission. We conclude that a two-temperature model is clearly inferior to the scattering model in explaining the observed line emission.

Radiative pumping by a strong infrared continuum is another possibility that needs to be considered as an alternative excitation mechanism and a way to avoid the scattering scenario by introducing non-LTE effects. This would produce a single vibrational temperature (Scoville et al. 1980). However it does not explain why the rotational and vibrational temperatures seem to be identical. Also, luminosities larger than 10^3 $L_\odot$ are required to effectively pump CO molecules to the second vibrational level or higher at distances from the central source beyond 1 AU (Scoville et al. 1980). Using the 1-dimensional Monte-Carlo radiative transfer code from Schöier (2000) illustrates the effects of radiative excitation on the line populations. The simplest possible model for radiative excitation assumes a blackbody with a luminosity $L = 25$ $L_\odot$ at the center of a single density spherical and static envelope. The blackbody temperature is taken to be the colour temperature of the continuum around 4.7 μm, determined from the M-band spectrum to 420 K. The radius used is the observed 320 AU, the gas kinetic temperature is assumed to be a power law beginning at the surface of the central source. The molecular constants are taken from Schöier et al. (2002). This leaves the gas density as

Table 2. Best fitting models for GSS 30 IRS1.

Model	Lines used	T [K]	N(CO) [cm^{-2}]	Red. χ^2
Optically thin direct calculation	^{13}CO v = 1–0 + ^{12}CO v = 2–1	500 ± 25	$4 \pm 1 \times 10^{14}$	1.4
Full radiative transfer	^{13}CO v = 1–0	degenerate	degenerate	0.85
Full radiative transfer	^{12}CO v = 1–0 + ^{12}CO v = 2–1	725 ± 50	$2.5 \pm 1 \times 10^{13}$	2.38
Full radiative transfer with scattering	All	515 ± 10	$1.5 \pm 0.5 \times 10^{18}$	1.29

the only free parameter, which basically determines the optical depth of the lines and consequently the importance of line trapping effects. The model calculations show that a density of at least $n_{\mathrm{H_2}} \sim 10^6$ cm^{-3} is needed to reproduce the approximate flux level of the ^{12}CO v = 1–0 lines. The vibrational excitation temperature is largely determined by the continuum flux level at 4.7 μm and therefore by the luminosity and to a smaller extent the temperature of the radiating source. Since the dominating mechanism for populating the v = 2 level is via the v = 1 level, and since both the v = 2–1 and v = 1–0 transitions are placed in the same narrow wavelength region, the radiative excitation rates are strongly dependent on local photon density in the 4.7 μm region. Consequently, as long as the direct route through the v = 2–0 overtone transitions around 2.35 μm is not important, the vibrational level population depends on the temperature of the input radiation field only through the flux level at 4.7 μm. At the adopted luminosity, the ^{12}CO v = 2–1 line fluxes are two orders of magnitude too low, reflecting an excitation temperature of 400 K. To significantly populate the second vibrational levels, a luminosity of at least 10^3 $L_\odot$ is required, in agreement with Scoville et al. (1980). Finally, the population of the rotational levels shows significant departures from a Boltzmann distribution, especially when line trapping becomes important. Altogether, this indicates that radiative pumping as an excitation mechanism in the case of GSS 30 IRS1 is unlikely.

Finally, the possibility that the lines are continuum emission which is resonance scattered in CO transitions should be considered. It is known that this takes place in the case of asymptotic giant branch stars, e.g. in the case of Mira (Ryde & Schöier 2001). However, since this mechanism probes the scattering gas rather than the emitting medium, it will not solve the discrepancy. Also it would require that the gas at a distance of 320 AU from the central source has a single temperature of 500 K, which seems highly unlikely.

4.4. Hydrogen recombination lines and mass loss rate

There are a number of hydrogen recombination lines common to YSOs (Pfβ, Brα, Pfδ) present in the 3–5 μm region, which are usually taken as an indicator of accretion activity. This is particularly true in the case of low mass young stars, where the hard radiation from the boundary layer between disk and star is needed to produce the ionizing radiation, since the central star is not hot enough. Because these lines have broad wings (3–500 km s^{-1}), they are often interpreted as coming from a strong stellar wind, which may be the engine of an outflow. The possibility that the CO gas could be associated with a wind or molecular outflow should therefore be explored. If associated with a stellar wind, the lines could be formed either as cooling emission from the gas as molecules are reformed or as emission from a shock as the wind collides with the circumstellar envelope or disk. It is known that no large scale outflow is present which could be produced by any of the three stars in the cluster, but there is some evidence of an expanding core surrounding the cluster from interferometric observations of rotational ^{13}CO and C^{18}O lines (Zhang et al. 1997).

Hydrogen recombination lines emitted from a plasma moving at supersonic speeds can be modeled in the Sobolev approximation (Sobolev 1960), which is valid when the thermal line broadening is much smaller than the wind speed. This formalism has been treated for spherical ionized winds in LTE from evolved stars in Castor (1970) and Krolik & Smith (1981), and for Herbig AeBe stars in Nisini et al. (1995). Using this formalism an ionized mass loss rate can be estimated for the star if a wind origin for the hydrogen lines is assumed. The extinction corrected line intensities for the hydrogen recombination lines observed in GSS 30 IRS1 are tabulated in Table 3 along with the mass loss rates derived from each line. The line ratios and the mass loss rate are not sensitive to the temperature, so a constant electron temperature of 10^4 K has been assumed. Finally, it is assumed that the central star does not shadow a significant part of the radiation from the wind. Changing the model parameters, i.e. the temperature and the size of the ionized region, with a factor of two changes the mass loss rate with a factor of two at most. The velocity structure is such that the wind starts at the surface of the star with 20 km s^{-1} and rises quickly to 450 km s^{-1} to fit the observed *FWHM* of the Pfβ line. The exact shape of the velocity structure is otherwise not significant for the derived mass loss rate.

We find that an ionized mass loss rate of 1.7×10^{-6} $M_\odot$ year^{-1} = 0.6 $M_\oplus$ year^{-1} is consistent with the two observed Pfund lines. The Brα line is too faint for this mass loss rate, which may indicate deviations from LTE. We can rule out that it is an effect from a poor extinction correction since the Brα line lies between the Pfβ and Pfδ lines in wavelength. The most serious problem with this model is likely that very little is known about the structure of winds from low mass embedded YSOs; in particular, the ionization structure will depend directly on energetic processes which are poorly understood, such as accretion activity or interactions of the circumstellar matter with strong magnetic fields. Also, if the wind is predominantly neutral, then the total mass loss rate will be much higher than the ionized mass loss rate and will become inconsistent with the non-detection of an outflow. It is possible that other mechanisms such as accretion flows must be considered

Table 3. Hydrogen recombination lines observed in GSS 30 IRS1.

Transition	Line intensity [erg cm^{-2} s^{-1}]	*FWHM* [km s^{-1}]	Mass loss rate [$M_\odot$ year^{-1}]
Pfβ	$1.3 \pm 0.5 \times 10^{-13}$	450 ± 50	1.7×10^{-6}
Brα	$1.6 \pm 0.2 \times 10^{-13}$	$\lesssim$500	0.8×10^{-6}
Pfδ	$6.0 \pm 1.0 \times 10^{-14}$	$\lesssim$500	1.8×10^{-6}

for the formation of recombination lines from low mass young stars. The hydrogen lines are therefore not likely to provide any strong constraints on the emitting CO gas and a detailed discussion on the hydrogen emission is outside the scope of this paper.

5. Discussion

In summary, to determine the origin of the CO gas emission it must be explained why only a single well-defined temperature is needed. Which mechanism can heat up to 100 $M_\oplus$ of gas to a unique temperature of 500 K, yet keep the intrinsic line width less than 30 km s^{-1}? Finally, why is no other similar embedded source from the literature showing the same strong CO ro-vibrational emission as GSS 30 IRS1?

5.1. Outflow?

If the warm CO gas resides in the wind/outflow component of the circumstellar environment then an estimate of the time needed to create it can be found from the mass loss rate derived in Sect. 4.4 under the assumption that the wind is predominantly ionized. A mass between 3 and 100 $M_\oplus$ corresponds to a production time of minimally 5 years and maximally a few centuries, while the most likely time is about one century. It seems unlikely that hot, ionized material emitted over a longer period should thermalize at a single temperature. Also, an outflow origin of the line emission would produce broad wings in the lines, which is not observed. If the wind is predominantly neutral, the resulting mass loss rate would be so high that a clear outflow should have been detected.

5.2. Inner disk?

Another possibility is that the emission is produced by warm thermalized gas in the disk itself. Since more evolved T Tauri disks are known to exhibit similar CO emission, although with smaller intensities, it is conceivable that we are seeing an equivalent process in the case of a younger disk. A typical circumstellar disk around a low mass young star is often observed to have a mass of a few times the minimum solar nebula, i.e. $M_{\rm disk} \sim$ a few 0.01 $M_\odot$ (André & Montmerle 1994; Osterloh & Beckwith 1995). The disk mass for GSS 30 IRS1 inferred by the 1.3 mm continuum emission is $M_{\rm disk} = 0.03\ M_\odot$ (André & Montmerle 1994). In hydrostatic equilibrium, a disk irradiated by the central star has a surface density $\Sigma \sim R^{-3/2}$ (Chiang & Goldreich 1997). If viscous dissipation in the disk is taken into account the surface density attains a flatter R-dependency, $\Sigma \sim R^{-1}$. In both cases the accumulated disk mass reaches the observed 10–100 $M_\oplus$ between 2 and 10 AU from the central star. A single temperature of 515 K is however not consistent with the disk models, which prescribe a large range in temperatures with a small 1000–2000 K component within a few stellar radii to an extended 100–200 K component within a few AU of the central star. However, in no models for passive circumstellar disks is it expected that the disk exhibits a single temperature, indeed quite the contrary is the case. Furthermore, Keplerian rotation within a few AU would produce observable line broadening. The narrow lines could only be explained if we are seeing light emitted vertically from the plane of the disk before being scattered into the line of sight, effectively removing the effects of rotation.

5.3. Accretion shock?

A final option is that the emission lines are cooling lines from post-shocked dense gas. Vibrational H_2 emission is one of the principal tracers of low density ($n_{H_2} \lesssim 10^7$ cm^{-3}) shocked gas. As mentioned in Sect. 3.1 the (0–0) S(9) line of H_2 at 4.695 μm is seen in our M-band spectrum, while no H_2 lines are seen in the K-band spectrum of GSS 30 IRS1 by Greene & Lada (1996) although no upper limit is given. Assuming that the observed H_2 (0–0) S(9) line is thermalized at the CO temperature, the required molecular gas mass is 5 $M_\oplus$. This is assuming that the H_2 emission is seen directly and is not corrected for extinction, since the extinction is hard to estimate for embedded stars. A typical Ophiuchus extinction of $A_V = 25$ mag (Teixeira & Emerson 1999) will increase the molecular gas mass by a factor of 2. If the emission in the H_2 line is scattered in the same way as the CO emission all values must be multiplied by ϵ. If the H_2 emission is thermalized at 515 K and directly observed then the integrated line flux expected for the 2.12 μm (1–0) S(1) line is 7.5×10^{-13} erg cm^{-2} s^{-1}, which should be observable. If the H_2 lines are scattered into the line of sight with an efficiency of ϵ, then no H_2 lines should be visible in the M-band. Consequently, the H_2 line does not seem to be directly associated with the same gas emitting the CO lines since it is at least a factor of 10 too bright, but it may be an indication of a warmer component or the line may be pumped. Sensitive observations of H_2 lines in the K- and L-band are needed to unambigously determine the origin of the molecular hydrogen emission.

Neufeld & Hollenbach (1994) show that if a dense gas of $10^{7.5} < n_{H_2} < 10^{12}$ cm^{-3} is shocked, the vibrational emission from H_2 is significantly suppressed partly because the shock dissociates the H_2 molecules and partly because the reforming molecules can easily be collisionally de-excited in the dense post-shock gas. The main coolants will be rotational and

vibrational lines from H_2O, OH and CO. This is valid for a wide range of shock velocities $5 < v_s < 100$ km s^{-1} as long as the shock is of jump-type. A *J*-shock occurs in any case for $v_s \gtrsim 30$ km s^{-1} and for smaller shock velocities if the magnetic field is weak or if the length scale over which the shock occurs is small compared to the length scale for acceleration of charged particles. Furthermore, the theoretical post-shock temperature structure gives an interesting prediction. A *J*-shock will dissociate the gas at the shock front. The gas then cools slowly from 10^5 K principally through the Lyα-line until CO forms at around 7000 K and $N(\mathrm{HI}) \sim 10^{21}$ cm^{-2}. Once the CO molecules are available the gas cools quickly to about 500 K through the CO vibrational lines, where a constant temperature plateau is maintained due to the release of chemical potential energy as H_2 is formed which is balanced against the thermalized vibrational emission from molecules. The plateau occurs at an atomic hydrogen column density of 10^{21}–10^{22} cm^{-2}, which in the model by Neufeld & Hollenbach (1994) corresponds to a CO column density of 3×10^{17}–3×10^{18} cm^{-2}. It is stressed that the slower C-shock scenario was not treated in such high density models, and it may produce similar cooling lines. Further modelling is needed to exclude a slow shock. It is evident that the model values are remarkably similar to the values observed in GSS 30 IRS1 with temperature $T_{\mathrm{gas}} = 515$ K and column density $N(\mathrm{CO}) = 2 \times 10^{18}$ cm^{-2}. However, it is unclear why no hot 5000–7000 K component in the fundamental CO band is observed, which is also expected from the shock. Also no overtone emission is seen in the *K*-band spectrum of Greene & Lada (1996). One plausible explanation is that the accretion activity is highly variable and that the hot component is only seen as the shock is occurring while the warm thermalized gas is seen in the post-shock medium. This would be supported by the variable water maser emission. The single observed H_2 line is not inconsistent with an accretion shock although it is too bright to be associated with a dense shocked gas and may only be an indication of a warmer less dense component.

As described in Neufeld & Hollenbach (1994), the most likely site for a dense shock in an embedded YSO is in a circumstellar disk which is accreting matter. When infalling matter is colliding with the disk at supersonic velocities, a *J*-shock is expected to occur at the surface of the disk. If the accretion velocities are too low to produce a *J*-shock, the molecules will not be dissociated and the observed temperature plateau will not be present. The main uncertainty is if the high infall velocities required to create a dissociative shock are possible. However, infall velocities of 10 km s^{-1} within 10 AU are reasonable (Cassen & Moosman 1981). Therefore, if the dissociative accretion shock scenario holds, the intrinsic line widths are *predicted* to be larger than or very close to 10 km s^{-1}. An accretion shock at a large distance ($\gtrsim$10 AU) from the central star is consistent with the observation that the line emitting region is physically separated from the continuum emitting region. A shock will not heat a large amount of dust and the continuum emission, which has a colour temperature of about 700 K, is likely to be produced by irradiated dust within 1 AU of the star.

Other observable tracers of a shock in a dense medium are the ro-vibrational lines from the H_2O ν_2 bending mode around 6 μm as well as the vibrational transitions of OH, all of which are unavailable from ground-based instruments. However, they may be detected by the upcoming Stratospheric Observatory For Infrared Astronomy (SOFIA) mission.

The possible dissociation of the molecules has important consequences for the chemistry in the inner disk. If the emission is indeed coming from an accretion shock, and if a significant amount of matter passes through the shock, it will significantly affect the models of chemical evolution of the innermost parts of disks around low mass YSOs, by evaporating ice mantles and inducing high temperature chemistry.

6. Summary

In this paper, we have analyzed the 4.5–4.8 μm spectrum of the embedded young stellar object GSS 30 IRS1 in the ρ Ophiuchus core. The observed emission lines from the ro-vibrational transitions of CO are fitted with a simple full radiative transfer 1D model. It is found that the line emission must be scattered on a bipolar cavity in order to simultaneously account for the size of the observed emitting region, the absolute flux level of the lines and the ratio of ^{12}CO to ^{13}CO lines. In this case the emission is well fitted by a single temperature gas with $T = 515 \pm 10$ K and a column density of $N(\mathrm{CO}) = 2 \pm 0.5 \times 10^{18}$ cm^{-2}. Furthermore, assuming a two-temperature distribution of the gas does not yield satisfactory fits.

The observed emission line spectrum can be best explained by the presence of a *J*-shock in a dense medium, although other possible scenarios cannot be ruled out. Most likely the shock is produced by the accretion of gas onto a dense disk within a few tens of AU from the star as predicted by Neufeld & Hollenbach (1994). Only this scenario explains why a large amount of CO gas is thermalized at a single temperature of ~500 K and why the emission lines are so narrow.

Acknowledgements. The authors wish to thank the VLT staff for all their help in obtaining the observations and in particular Chris Lidman for many helpful comments on the data reduction. We also acknowledge the many constructive suggestions made by an anonymous referee, which helped improve the quality of this paper. This research was supported by the Netherlands Organization for Scientific Research (NWO) grant 614.041.004, the Netherlands Research School for Astronomy (NOVA) and a NWO Spinoza grant.

References

André, P., & Montmerle, T. 1994, ApJ, 420, 837
Bensch, F., Pak, I., Wouterloot, J. G. A., Klapper, G., & Winnewisser, G. 2001, ApJ, 562, 185
Blake, G. A., Boogert, A. C. A., & Kessler, J. 2002, ApJ, in prep
Bontemps, S., André, P., Kaas, A. A., et al. 2001, A&A, 372, 173
Boogert, A. C. A., Hogerheijde, M. R., & Blake, G. A. 2002, ApJ, 568 [astro-ph/0112163]
Boogert, A. C. A., Tielens, A. G. G. M., Ceccarelli, C., et al. 2000, A&A, 360, 683
Carr, J. S. 1989, ApJ, 345, 522
Carr, J. S., Mathieu, R. D., & Najita, J. R. 2001, ApJ, 551, 454
Cassen, P., & Moosman, A. 1981, Icarus, 48, 353
Castor, J. I. 1970, MNRAS, 149, 111

Chiang, E. I., & Goldreich, P. 1997, ApJ, 490, 368
Chrysostomou, A., Clark, S. G., Hough, J. H., et al. 1996, MNRAS, 278, 449
Chrysostomou, A., Ménard, F., Gledhill, T. M., et al. 1997, MNRAS, 285, 750
Claussen, M. J., Wilking, B. A., Benson, P. J., et al. 1996, ApJS, 106, 111
Draine, B. T. 1985, ApJS, 57, 587
Draine, B. T., & Lee, H. M. 1984, ApJ, 285, 89
Elias, J. H. 1978, ApJ, 224, 453
Grasdalen, G. L., Strom, K. M., & Strom, S. E. 1973, ApJ, 184, L53
Greene, T. P., & Lada, C. J. 1996, AJ, 112, 2184
Greene, T. P., Wilking, B. A., André, P., Young, E. T., & Lada, C. J. 1994, ApJ, 434, 614
Krolik, J. H., & Smith, H. A. 1981, ApJ, 249, 628
Leous, J., Feigelson, E. D., André, P., & Montmerle, T. 1991, ApJ, 379, 683
Mitchell, G. F., Allen, M., Beer, R., et al. 1988, ApJ, 327, 17
Mitchell, G. F., Maillard, J.-P., Allen, M., Beer, R., & Belcourt, K. 1990, ApJ, 363, 554
Najita, J., Carr, J. S., Glassgold, A. E., Shu, F., & Tokunaga, A. T. 1996, ApJ, 462, 919
Najita, J. R., Edwards, S., Basri, G., & Carr, J. 2000, in Protostars and Planets IV (The University of Arizona Press), 457
Neufeld, D. A., & Hollenbach, D. J. 1994, ApJ, 428, 170
Nisini, B., Milillo, A., Saraceno, P., & Vitali, F. 1995, A&A, 302, 169
Osterloh, M., & Beckwith, S. V. W. 1995, ApJ, 439, 288
Pendleton, Y. J., Tielens, A. G. G. M., & Werner, M. W. 1990, ApJ, 349, 107
Reipurth, B., & Aspin, C. 1997, AJ, 114, 2700
Rothman, L. S., Rinsland, C. P., Goldman, A., et al. 1998, J. Quant. Spectrosc. Radiat. Trans., 60, 665
Ryde, N., & Schöier, F. L. 2001, ApJ, 547, 384
Schöier, F. L., Ryde, N., & Olofsson, H. 2002, A&A, 391, 577
Schöier, F. L. 2000, Ph.D. Thesis, Department of Astronomy, Stockholm University
Scoville, N. Z., Krotkov, R., & Wang, D. 1980, ApJ, 240, 929
Tamura, M., Sato, S., Suzuki, H., Kaifu, N., & Hough, J. H. 1990, ApJ, 350, 728
Teixeira, T. C., & Emerson, J. P. 1999, A&A, 351, 292
Teixeira, T. C., Emerson, J. P., & Palumbo, M. E. 1998, A&A, 330, 711
Thompson, R. I. 1989, ApJ, 344, 799
van Dishoeck, E. F., Dartois, E., Thi, W. F., et al. 2001, in The Origins of Stars and Planets, ed. J. Alves, & M. McCaughrean (Springer Verlag) [astro-ph/0110465]
Wilking, B. A., Lada, C. J., & Young, E. T. 1989, ApJ, 340, 823
Zhang, Q., Wooten, A., & Ho, P. T. P. 1997, ApJ, 475, 713